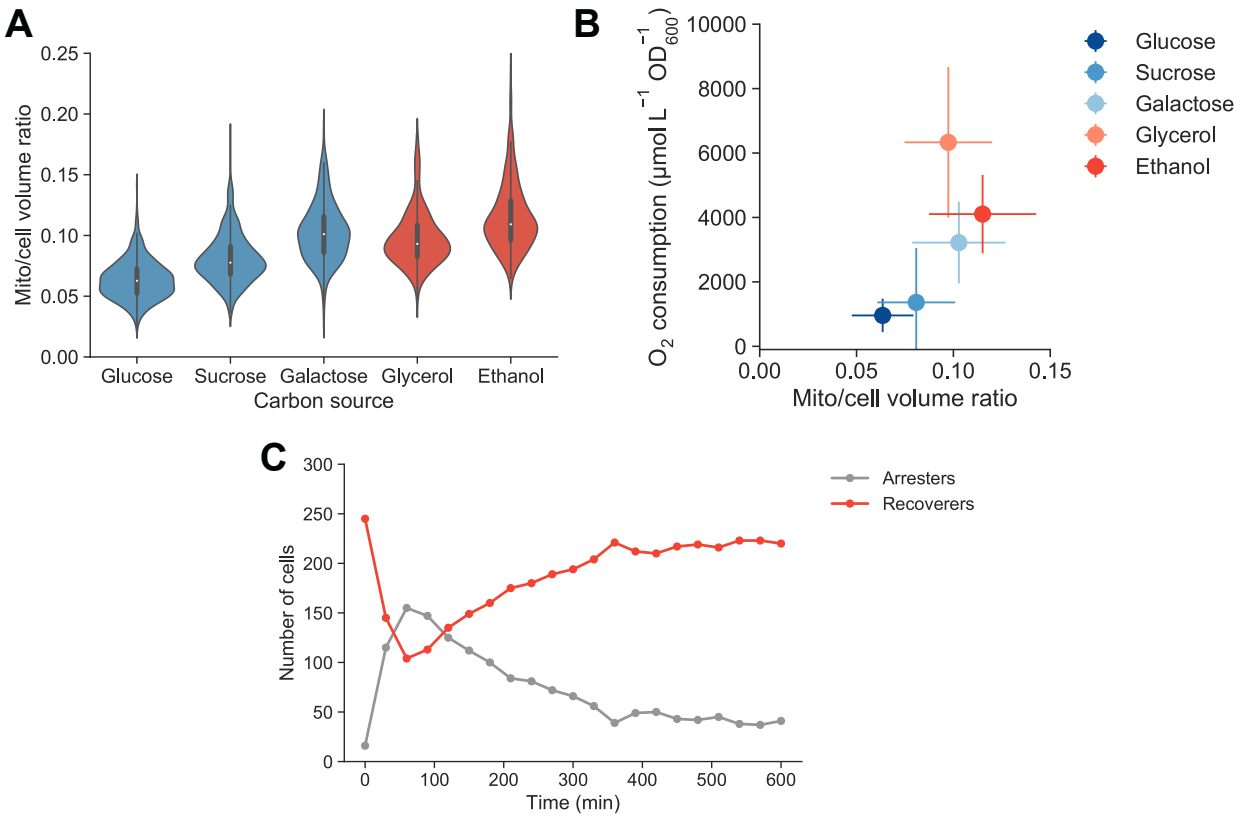

Figure S1. Mitochondrial structure and metabolic output vary across environments. Related to Figure 1.

(A) The ratio of mitochondrial volume to total volume of cells expressing mitochondrially targeted mNeonGreen (yLB126) and growing exponentially in synthetic media containing either 2% glucose, 2% sucrose, 2% galactose, 3% glycerol, or 2% ethanol, examined by microscopy. N ≥ 316 cells collected across three biological replicates. Blue: fermentable carbon sources, red: non-fermentable carbon sources.

(B) Oxygen consumption rates of yLB1 were measured in sealed cell culture plates equipped with a fluorescent oxygen sensor while cells grew exponentially in synthetic media containing varying carbon sources, conducted in parallel with volumetric measurements collected by microscopy in *(A)*. Rates normalized by doubling time of each strain, measured in tandem. Error bars indicate one standard deviation.

(C) Cells were classified as arrested or recovered on the basis of mitochondrial network morphology (sphericity index > 0.7 or ≤ 0.7, respectively) for 10 hr following glucose withdrawal. N = 261 cells collected across three independent biological replicates. A minority of cells displayed no mitochondrial collapse on the time intervals at which images were acquired (15 min). We are uncertain whether these cells experienced a temporary mitochondrial shock which is not detectable at this temporal resolution, and thus in our downstream analyses we simply classify cells as either recovering or arresting on the basis of their ultimate fate.

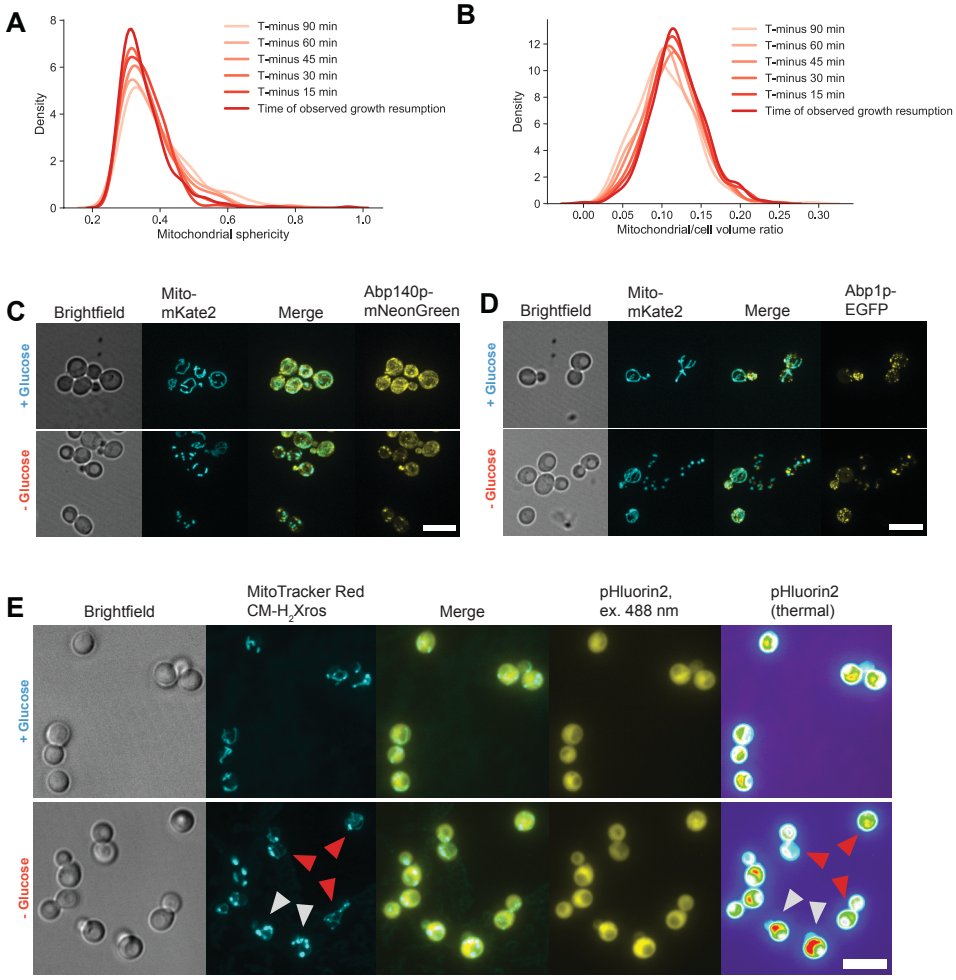

Figure S2. Structural defects associated with growth arrest during sudden starvation. Related to Figure 2.

(A)-(B) Dynamics of mitochondrial sphericity *(A)* and mitochondrial/cell volume ratio *(B)* in N = 357 cells in the 90 min prior to detectable growth resumption.

(C)-(D) Representative images of cells co-expressing a mitochondrial marker in tandem with actin cable-associated protein Abp140p (yLB69) *(C)*, or endocytic actin patch marker Abp1p (yLB45) *(D)*, growing in synthetic media containing high glucose and following glucose washout. Scale bars, 10 µm. The two actin-binding proteins largely maintain their distribution in cells where mitochondria are tubular and lose it in cells whose mitochondria collapse.

(E) Images of cells expressing ratiometric pHluorin2 (yLB397) and stained with MitoTracker Red CM-H_2Xros, in synthetic medium containing high glucose and post-glucose deprivation. MitoTracker Red images are presented as maximum-intensity z-projections for clarity of mitochondrial morphology; pHluorin2 images consist of the summed intensity across all z-slices for retention of expression information. Excitation of pHluorin2 at 488 nm produces a stronger fluorescence signal as pH decreases. Far right panels depict pHluorin2 signal as a thermal heat map for ease of comparison. Red and gray arrows indicate examples of cells with tubular and collapsed mitochondria, respectively. Scale bar, 10 µm.

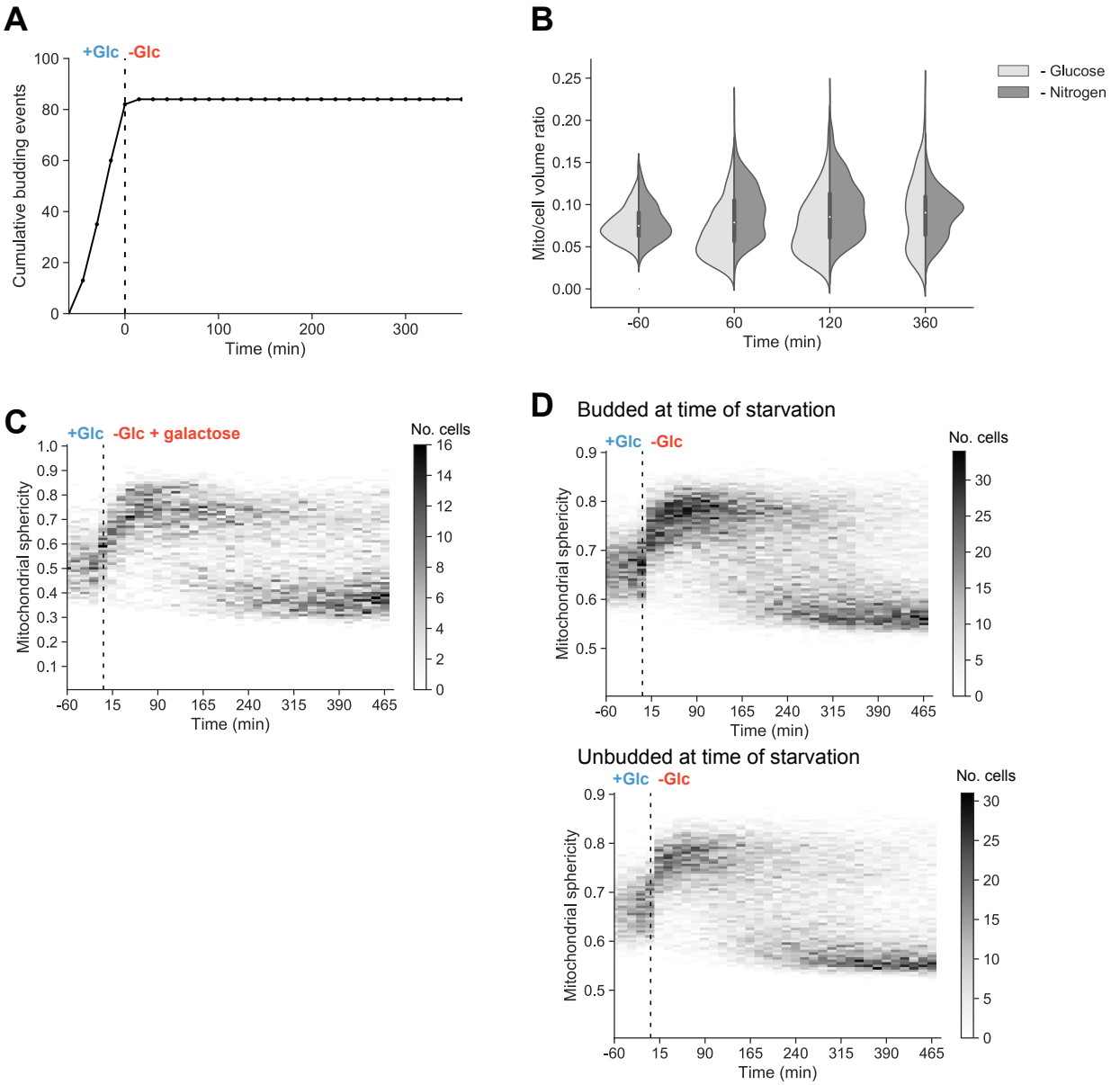

Figure S3. Mitochondrial starvation heterogeneity is unique to glucose deprivation and is not explained by cell cycle starvation heterogeneity. Related to Figure 3.

(A) Cumulative budding events occurring prior to and following abrupt glucose withdrawal in a microfluidic chamber, with growth dynamics observed by microscopy. Prototrophic cells (yLB128) were grown in synthetic media lacking amino acids, with and without glucose. Data are an aggregation of three independent biological replicates.

(B) Distributions of mitochondrial to total cell volume ratio in cells (yLB128) growing in synthetic media without amino acids, before or following the shift to identical media lacking either glucose or nitrogen (ammonium sulfate), performed at time 0 min. N ≥ 360 cells.

(C) Heat map depicting the distribution of mitochondrial sphericity values for cells (yLB126) growing in a microfluidics unit in synthetic media containing high glucose,

before and after a nutrient shift to identical media containing high galactose in lieu of glucose, performed at time 0 min. Intensity reflects the number of cells possessing a sphericity index within a given 0.01-sphericity-unit bin. N = 354 cells.
(D) Heat maps of mitochondrial sphericity for yLB126, before and during glucose starvation, with data partitioned by budded or unbudded status at the moment of glucose washout. N ≥ 404 cells.

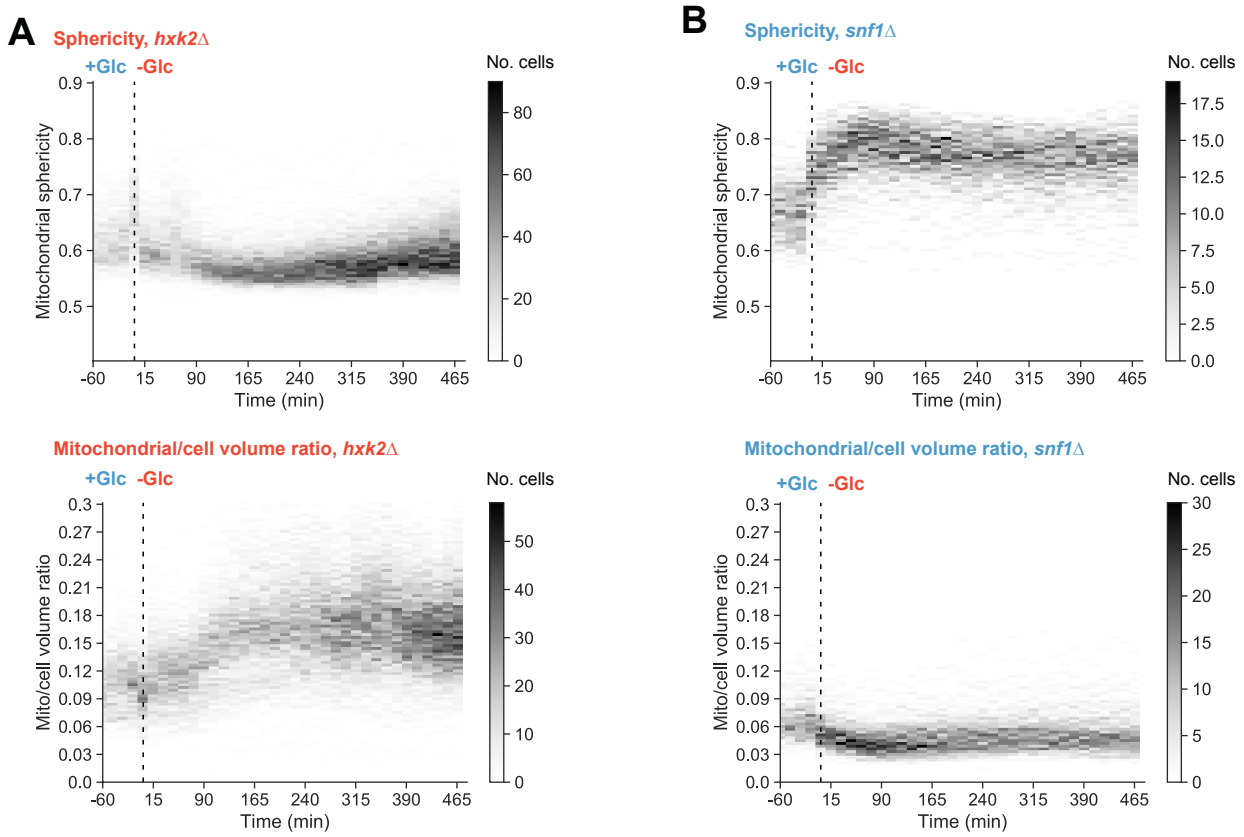

Figure S4. Disruption of glucose signaling and utilization abrogate bimodal behavior during starvation. Related to Figure 4.

(A) Time-resolved heat maps of mitochondrial-to-total cell volume ratio and sphericity in N = 523 *hxk2Δ* cells (yLB146), before and during acute glucose starvation occurring at 0 min. Compare to Figures 1G and 1H.

(B) Time-resolved heat maps of mitochondrial-to-total cell volume ratio and sphericity in N = 342 *snf1Δ* cells (yLB168), before and during acute glucose starvation.

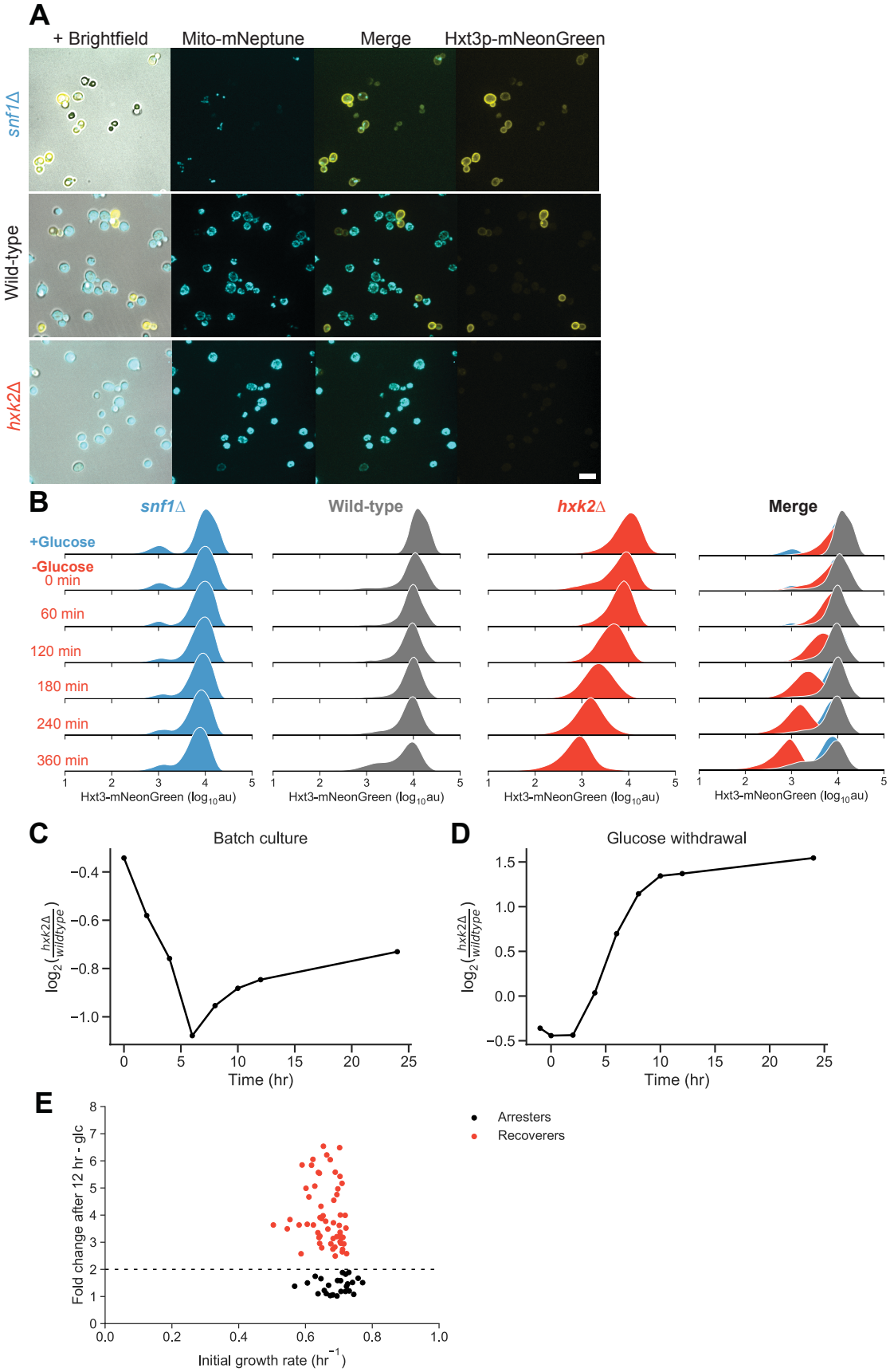
A
+ Brightfield
Mito-mNeptune
Merge
Hxt3p-mNeonGreen
snf1Δ
Wild-type
hxk2Δ
B
snf1Δ
Wild-type
hxk2Δ
Merge
+Glucose
-Glucose
0 min
60 min
120 min
180 min
240 min
360 min
Hxt3-mNeonGreen (log10au)
C
Batch culture
log2(hxk2Δ/wildtype)
Time (hr)
D
Glucose withdrawal
log2(hxk2Δ/wildtype)
Time (hr)
E
Arresters
Recoverers
Fold change after 12 hr - glc
Initial growth rate (hr-1)

Figure S5. Fast adaptation to glucose withdrawal confers a reciprocal fitness cost under well-fed conditions. Related to Figure 5.

(A) Representative images of cells co-expressing fluorescently labeled Hxt3p-mNeonGreen and mitochondrial matrix-targeted mito-mNeptune in *snf1Δ* (yLB299), *hxk2Δ* (yLB297), or wild-type (yLB256) mutant backgrounds following 24 hr of glucose deprivation. While *hxk2Δ* mutants display uniform mitochondrial network increase and loss of Hxt3p signal and *snf1Δ* uniformly retain Hxt3p-mNeonGreen and have fragmented mitochondria (save for some cells that died during prolonged starvation, evident from their shriveled size and increase autofluorescence), the wild-type population is a heterogeneous distribution of Hxt3p-positive cells with mitochondrial fragmentation and Hxt3p-negative cells with large mitochondrial networks. Scale bar, 10 μm.

(B) Hxt3p-mNeonGreen intensity measured by flow cytometry in wild-type, *snf1Δ*, and *hxk2Δ* cells growing in the presence of high glucose and deprived of glucose for the indicated time intervals. Distributions consist of three biological replicates of N = 40,000 cells each.

(C)-(D) Cultures were initiated with equal proportions of wild-type (yLB365) and *hxk2Δ* (yLB373) cells, each expressing distinct fluorescent markers, in synthetic medium containing high glucose. The proportions of wild-type and *hxk2Δ* cells were measured during continued cultivation in high glucose *(C)* and following sudden glucose withdrawal *(D)*. N = 40,000 cells measured by flow cytometry at each time point. In (C), the fraction of *hxk2*Δ cells reaches a minimum at the onset of the diauxic shift, which occurs when all glucose has been fermented, and then rises as cells begin to respire.

(E) Pre-starvation growth rate of microcolonies founded by single cells plotted against the change in the cell lineage's size following abrupt glucose withdrawal from the media. Lineages are assigned to two states, recoverers (red) and arresters (black), by their success or failure in doubling in size over the first 12 hr of glucose starvation.

Strain name	Genotype description
yLB1	*W303 MATa can1-100 leu2-3,112 his3-11,15 ura3-1 BUD4-S288C RAD5 TRP*
yLB41	*yLB1 his3::pADH1-preSu9-link-mKate2-ADH1term-HIS3 SEC63-EGFP-KAN*
yLB45	*yLB1 his3::pADH1-preSu9-link-mKate2-ADH1term-HIS3 ABP1-EGFP-KAN*
yLB69	*yLB1 his3::pADH1-preSu9-link-mKate2-ADH1term-HIS3 ABP140-mNeonGreen-KAN*
yLB73	*yLB1 rho^0*
yLB113	*W303 MATa can1-100 his3::pADH1-preSu9-link-EGFP-ADH1term-HIS3 BUD4-S288C RAD5 TRP*
yLB126	*yLB1 his3::pADH1-preSu9-link-mNeonGreen-ADH1term-HIS3*
yLB128	*W303 MATa can1-100 his3::pADH1-preSu9-link-mNeonGreen-ADH1term-HIS3 BUD4-S288C RAD5 TRP*
yLB134	*yLB1 his3::pADH1-preSu9-link-mNeonGreen-ADH1term-HIS3 dnm1::KAN*
yLB145	*yLB1 hxk2::NAT*
yLB146	*yLB126 hxk2::NAT*
yLB167	*yLB1 snf1::KAN*
yLB168	*yLB126 snf1::KAN*
yLB180	*yLB126 mig1::NAT mig2::KAN*
yLB181	*yLB1 mig1::NAT mig2::KAN*
yLB194	*yLB1 reg1::KAN*
yLB196	*yLB126 reg1::KAN*
yLB219	*yLB1 his3::pADH1-preSu9-link-ratiometric pHluorin-HIS3 ura3-1*
yLB232	*yLB1 snf3::KAN rgt2::NAT*
yLB233	*yLB126 snf3::KAN rgt2::NAT*
yLB256	*yLB1 his3::pADH1-preSu9-link-mNeptune-ADH1term-HIS3 HXT3-mNeonGreen-CgLEU2*
yLB297	*yLB256 hxk2::NAT*
yLB299	*yLB256 snf1::KAN*
yLB365	*yLB1 his3::pACT1-mNeptune-ADH1t-HIS3*
yLB373	*yLB1 his3::pACT1-mNeonGreen-ADH1t-HIS3 hxk2::NAT*
yLB397	*yLB1 his3::pACT1-ratiometric pHluorin-ADH1term-HIS3*
yLB412	*yLB397 his3::pACT1-ratiometric pHluorin-ADH1term-HIS3 snf1::KAN*
yLB416	*yLB397 his3::pACT1-ratiometric pHluorin-ADH1term-HIS3 hxk2::NAT*
yLB432	*W303 MATa can1-100 leu2-3,112 his3-11,15 BUD4-S288C RAD5 TRP URA HXT3-mNeonGreen-SpHIS5 HXT7-mNeptune-CgLEU2*
yLB453	*BC187 HIS3::pHXT3-HXT3-link-mNeonGreen-ADH1t-KAN-HIS3*
yLB457	*Y12 HIS3::pHXT3-HXT3-link-mNeonGreen-ADH1t-KAN-HIS3*
yLB463	*YJM978 HIS3::pACT1-mNeptune-ADH1t-KAN-HIS3*
yLB467	*CEN.PK HIS3::pACT1-mNeptune-ADH1t-KAN-HIS3*
yLB470	*DBVPG1373 HIS3::pACT1-mNeptune-ADH1t-KAN-HIS3*
yLB474	*L-1374 HIS3::pACT1-mNeptune-ADH1t-KAN-HIS3*

yLB478	*BC187 HIS3::pACT1-mNeptune-ADH1t-KAN-HIS3*
yLB480	*YS2 HIS3::pACT1-mNeonGreen-ADH1t-KAN-HIS3*
yLB486	*Y12 HIS3::pACT1-mNeptune-ADH1t-KAN-HIS3*
yLB492	*K11 HIS3::pACT1-mNeptune-ADH1t-KAN-HIS3*
yLB494	*YPS606 HIS3::pACT1-mNeptune-ADH1t-KAN-HIS3*
yLB496	*UWOPS83-787.3 HIS3::pACT1-mNeptune-ADH1t-KAN-HIS3*

Table S1 Transgenic yeast strains used in this study. Related to STAR Methods.

Plasmid	**Base vector**	**Insert**	**Strains with insert integrated by homologous recombination**
pLB36	pRS403	pADH1-preSu9-link-mKate2-ADH1t-HIS3	yLB41, yLB45, yLB69
pLB39	pRS403	pADH1-preSu9-link-mNeptune-HIS3	yLB256, yLB297, yLB299
pLB52	pUC19	SEC63-link-yEGFP-ADH1t-KAN-3'SEC63	yLB41
pLB54	pUC19	ABP1-link-yEGFP-ADH1t-KAN-3'ABP1	yLB45
pLB57	pUC19	ABP140-link-mNeonGreen-ADH1t-KAN-3'ABP140	yLB69
pLB76	pRS403	pADH1-preSu9-link-mNeonGreen-ADH1t-HIS3	yLB126, yLB146, yLB168, yLB180, yLB196, yLB233
pLB104	pRS403	pADH1-preSu9-ratiometric pHluorin-ADH1t-HIS3	yLB219
pLB114	pUC19	HXT3-link-mNeonGreen-ADH1t-CgLEU2-3'HXT3	yLB256, yLB297, yLB299
pLB142	pUC19	HXT7-link-mNeptune-ADH1t-CgLEU2-3'HXT7	yLB432
pLB144	pUC19	HXT3-link-mNeonGreen-ADH1t-SpHIS5-5'HXT3	yLB432
pLB152	pRS403	pACT1-mNeptune-ADH1t-HIS3	yLB365
pLB153	pRS403	pACT1-mNeonGreen-ADH1t-HIS3	yLB373
pLB161	pRS403	pACT1-ratiometric pHluorin-ADH1t-HIS3	yLB397, yLB412, yLB416
pLB164	pRS403	pHXT3-HXT3-link-mNeonGreen-ADH1t-KAN-HIS3	yLB453, yLB457
pLB166	pRS403	pACT1-mNeonGreen-ADH1t-KAN-HIS3	yLB480
pLB168	pRS403	pACT1-mNeptune-ADH1t-KAN-HIS3	yLB463, yLB467, yLB470, yLB474, yLB478, yLB486, yLB492, yLB494, yLB496

Table S2 Plasmids used in the construction of transgenic yeast strains. Related to STAR Methods.